

Collaborative Filtering Based on Diffusion Models: Unveiling the Potential of High-Order Connectivity

Yu Hou
Yonsei University
Seoul, Republic of Korea
houyu@yonsei.ac.kr

Jin-Duk Park
Yonsei University
Seoul, Republic of Korea
jindeok6@yonsei.ac.kr

Won-Yong Shin*
Yonsei University
Seoul, Republic of Korea
wy.shin@yonsei.ac.kr

ABSTRACT

A recent study has shown that diffusion models are well-suited for modeling the generative process of user–item interactions in recommender systems due to their denoising nature. However, existing diffusion model-based recommender systems do not explicitly leverage high-order connectivities that contain crucial collaborative signals for accurate recommendations. Addressing this gap, we propose CF-Diff, a new diffusion model-based collaborative filtering (CF) method, which is capable of making full use of collaborative signals along with *multi-hop* neighbors. Specifically, the forward-diffusion process adds random noise to user–item interactions, while the reverse-denoising process accommodates our own learning model, named cross-attention-guided multi-hop autoencoder (CAM-AE), to gradually recover the original user–item interactions. CAM-AE consists of two core modules: 1) the attention-aided AE module, responsible for precisely learning latent representations of user–item interactions while preserving the model’s complexity at manageable levels, and 2) the *multi-hop cross-attention* module, which judiciously harnesses high-order connectivity information to capture enhanced collaborative signals. Through comprehensive experiments on three real-world datasets, we demonstrate that CF-Diff is **(a) Superior**: outperforming benchmark recommendation methods, achieving remarkable gains up to 7.29% compared to the best competitor, **(b) Theoretically-validated**: reducing computations while ensuring that the embeddings generated by our model closely approximate those from the original cross-attention, and **(c) Scalable**: proving the computational efficiency that scales *linearly* with the number of users or items.

CCS CONCEPTS

• **Information systems** → **Recommender systems**.

KEYWORDS

Collaborative filtering; cross-attention; diffusion model; high-order connectivity; recommender system.

*Corresponding author

Permission to make digital or hard copies of part or all of this work for personal or classroom use is granted without fee provided that copies are not made or distributed for profit or commercial advantage and that copies bear this notice and the full citation on the first page. Copyrights for third-party components of this work must be honored. For all other uses, contact the owner/author(s).
SIGIR '24, July 14–18, 2024, Washington, DC, USA
© 2024 Copyright held by the owner/author(s).
ACM ISBN 979-8-4007-0431-4/24/07.
<https://doi.org/10.1145/3626772.3657742>

ACM Reference Format:

Yu Hou, Jin-Duk Park, and Won-Yong Shin. 2024. Collaborative Filtering Based on Diffusion Models: Unveiling the Potential of High-Order Connectivity. In *Proceedings of the 47th International ACM SIGIR Conference on Research and Development in Information Retrieval (SIGIR '24)*, July 14–18, 2024, Washington, DC, USA. ACM, New York, NY, USA, 10 pages. <https://doi.org/10.1145/3626772.3657742>

1 INTRODUCTION

Diffusion models [15, 36] have become one of recent emerging topics thanks to their state-of-the-art performance in various domains, including computer vision [10, 15, 31], natural language processing [2, 33], and multi-modal deep learning [3, 32]. Diffusion models, categorized as deep generative models, gradually perturb the input data by adding random noise in the forward-diffusion process and then recover the original input data by learning in the reverse-denoising process, step by step. Due to their denoising nature, diffusion models align well with recommender systems, which can be viewed as a denoising process because user–item historical interactions are naturally noisy and diffusion models can learn to recover the original interactions based on corrupted ones [20, 43, 47]. Recent efforts have verified the effectiveness of diffusion models for sequential recommendations [21, 24, 48, 50], where the process of modeling sequential item recommendations mirrors the step-wise process of diffusion models. However, the application of diffusion models to recommender systems has yet been largely underexplored.

On one hand, one of the dominant techniques used in recommender systems is collaborative filtering (CF), where attention has been paid to model-based approaches including matrix factorization (MF) [19, 49] and deep learning [13, 14, 22, 29, 44, 51] (e.g., graph neural networks (GNNs) [13, 29, 44]). CF-based recommender systems have achieved great success in many real-world applications, due to their simplicity, efficiency, and effectiveness, while aiming to learn multi-hop relationships among users and items. For example, the message passing mechanism in GNNs, being increasingly used in the tasks of recommendation, captures collaborative signals in high-order connectivities by aggregating features of neighbors. Figure 1a illustrates the multi-hop neighbors used for CF with an example involving two users. It is seen that, although *User 1* and *User 3* have different direct interactions, they share similar 2-hop (*User 2*) and 3-hop (*Item 2*, *Item 5*) neighbors, which implies that *User 1* (resp. *User 3*) is highly likely to prefer *Item 4* consumed by *User 3* (resp. *Item 1* and *Item 3* consumed by *User 1*).

On the other hand, unlike the existing CF techniques using MF and GNNs, it is not straightforward to grasp how to exploit such high-order connectivity information from a *diffusion model’s* perspective, as shown in Figure 1b. Recent studies on diffusion model-

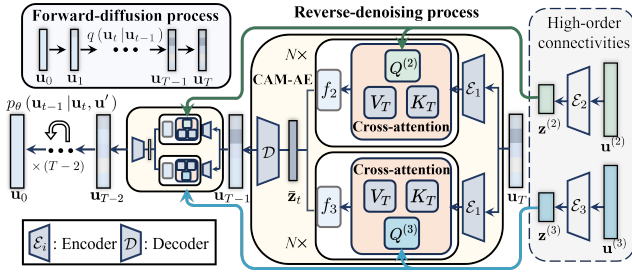


Figure 2: The schematic overview of CF-Diff when both 2-hop and 3-hop neighboring nodes are taken into account.

implicit feedback (such as a click or a view) between user u and item $i \in \mathcal{I}$, and 0 otherwise.¹

2.2 Overview of CF-Diff

We describe the methodology of CF-Diff, a new diffusion model-based CF method that is capable of reflecting high-order connectivity information, revealing co-preference patterns between users and items, for accurate recommendations. We recall that recent recommendation methods using diffusion models [21, 24, 40, 43, 48, 50] focus primarily on leveraging only the direct user–item interactions and overlook the collaborative signal in high-order connectivities during training. Our study aims to fill this gap by infusing high-order connectivity information into the proposed method, which poses two main design challenges that we mentioned earlier: preserving the learning model’s complexity at an acceptable level (C1) and learning complex high-order connectivities at a fine-grained level (C2).

To tackle these challenges, as a core module of CF-Diff, we develop an innovative learning model, CAM-AE. In the CAM-AE model, we propose to use a *multi-hop cross-attention* mechanism to infuse multi-hop neighborhood information from the target user during training, thereby enriching the collaborative signal, which however causes additional computational costs. To counter this, we next employ an *attention-aided AE* module, enabling to preserving the model’s complexity at manageable levels.

Note that diffusion models can be viewed as partitioning the denoising process of an AE into a series of finer sub-processes [9, 16], which can capture more delicate recovery details. Since CF-Diff is built upon such diffusion models, it naturally involves two distinct processes, namely the forward-diffusion process and the reverse-denoising process, achieved with a tailored neural network architecture in CAM-AE. The schematic overview of the CF-Diff method is illustrated in Figure 2, and each process in CF-Diff is summarized as follows.

- (1) **Forward-diffusion process (Section 2.3):** The forward diffusion, aligning with standard diffusion models, gradually adds Gaussian noise to the user–item historical interactions, as shown in the upper left part of Figure 2.
- (2) **Reverse-denoising process (Section 2.4):** We aim to gradually recover the original user–item interactions from noisy ones. This is achieved by using the proposed learning model, CAM-AE (to be specified Section 3), which infuses high-order

¹The unbolded u represents a user, while the bolded \mathbf{u} represents a certain user’s interaction vector as utilized in the proposed method.

connectivities to iteratively guide the reverse-denoising process. To bridge the historical one-hop interactions and multi-hop neighbors, our CAM-AE model integrates an attention-aided AE with a cross-attention architecture, progressively recovering user–item interactions by leveraging high-order connectivity information (see the right part of Figure 2).

2.3 Forward-Diffusion Process

We denote the initial state of a specific user $u \in \mathcal{U}$ as $\mathbf{u}_0 = \mathbf{u}$.² In the forward-diffusion process, we gradually insert Gaussian noise in the initial user–item interactions \mathbf{u}_0 over T steps, producing a sequence of noisy samples $\mathbf{u}_1, \dots, \mathbf{u}_T$, denoted as $\mathbf{u}_{1:T}$ (see Figure 2), which can be modeled as

$$q(\mathbf{u}_{1:T} | \mathbf{u}_0) = \prod_{t=1}^T q(\mathbf{u}_t | \mathbf{u}_{t-1}), \quad (1)$$

where

$$q(\mathbf{u}_t | \mathbf{u}_{t-1}) = \mathcal{N}(\mathbf{u}_t; \sqrt{1 - \beta_t} \mathbf{u}_{t-1}, \beta_t \mathbf{I}) \quad (2)$$

represents the transition of adding noise from states \mathbf{u}_{t-1} to \mathbf{u}_t via a Gaussian distribution [15, 36]. Here, $t \in \{1, \dots, T\}$ refers to the diffusion step; \mathcal{N} denotes the Gaussian distribution; and $\beta_t \in (0, 1)$ controls the Gaussian noise scales added at each time step t . To generate the noisy sample \mathbf{u}_t from $q(\mathbf{u}_t | \mathbf{u}_{t-1})$, we employ the reparameterization trick [18], expressed as $\mathbf{u}_t = \sqrt{1 - \beta_t} \mathbf{u}_{t-1} + \sqrt{\beta_t} \boldsymbol{\varepsilon}_{t-1}$, where $\boldsymbol{\varepsilon}_{t-1} \sim \mathcal{N}(\mathbf{0}, \mathbf{I})$. This process is iteratively applied until we obtain the final sample \mathbf{u}_T at time step T .

It is noteworthy that, in contrast to existing diffusion models, our approach focuses on adding noise to user–item interactions from a *single user’s* perspective, which originates from the nature of the denoising process in variational AE (VAE)-based CF [20].

2.4 Reverse-Denoising Process

In the reverse-denoising process, the estimation of the distribution $q(\mathbf{u}_{t-1} | \mathbf{u}_t)$ is technically not easy as it requires using the entire dataset. Therefore, a neural network model p_θ is employed to approximate such conditional probabilities [15]. Starting from \mathbf{u}_T , the reverse-denoising process gradually recovers \mathbf{u}_{t-1} from \mathbf{u}_t via the denoising transition step. However, only relying on user–item interactions do not ensure the high-quality recovery for CF-based recommendations, as high-order connectivity information plays an important role in guaranteeing state-of-the-art performance of CF, as shown in Figure 1a.

To address this, we integrate multi-hop neighbors of the target user u (denoted as \mathbf{u}') into our learning model, thereby enhancing recommendation accuracies. This differs from original diffusion models, which focus on denoising solely from noisy samples (*i.e.*, $p_\theta(\mathbf{u}_{t-1} | \mathbf{u}_t)$ in [15]). In other words, our approach not only denoises from noisy samples but also enriches the denoising process by exploiting high-order connectivities. The denoising transition via the Gaussian distribution is formulated as follows [15, 31]:

$$p_\theta(\mathbf{u}_{0:T}) = p(\mathbf{u}_T) \prod_{t=1}^T p_\theta(\mathbf{u}_{t-1} | \mathbf{u}_t, \mathbf{u}'), \quad (3)$$

²For notational convenience, since each user u experiences the forward-diffusion and reverse-denoising processes independently, we do not use the user index in u unless it causes any confusion.

where

$$p_{\theta}(\mathbf{u}_{t-1} | \mathbf{u}_t, \mathbf{u}') = \mathcal{N}(\mathbf{u}_{t-1}; \boldsymbol{\mu}_{\theta}(\mathbf{u}_t, \mathbf{u}', t), \boldsymbol{\Sigma}_{\theta}(\mathbf{u}_t, \mathbf{u}', t)). \quad (4)$$

Here, $\boldsymbol{\mu}_{\theta}(\mathbf{u}_t, \mathbf{u}', t)$ and $\boldsymbol{\Sigma}_{\theta}(\mathbf{u}_t, \mathbf{u}', t)$ are the mean and covariance of the Gaussian distribution predicted by the neural network with learnable parameters θ . Besides, to maintain training stability and simplify calculations, we ignore learning of $\boldsymbol{\Sigma}_{\theta}(\mathbf{u}_t, \mathbf{u}', t)$ in Eq. (4) and set $\boldsymbol{\Sigma}_{\theta}(\mathbf{u}_t, \mathbf{u}', t) = \beta_t \mathbf{I}$ by following [15]. After learning the mean $\boldsymbol{\mu}_{\theta}(\mathbf{u}_t, \mathbf{u}', t)$ in the model, we can obtain the recovered \mathbf{u}_{t-1} by sampling from $p_{\theta}(\mathbf{u}_{t-1} | \mathbf{u}_t, \mathbf{u}')$. This process is iteratively applied until we obtain an estimate of the original sample \mathbf{u}_0 .

The neural network architecture of CAM-AE is designed in the sense of judiciously infusing high-order connectivities in the reverse-denoising process. To this end, CAM-AE consists of two key components: 1) an *attention-aided AE* module precisely learns latent representations of the noisy user–item interactions, helping preserve the complexity manageable (solving the challenge C1), and 2) a *multi-hop cross-attention* module, which accommodates high-order connectivity information to facilitate the reverse-denoising process, thus capturing the enriched collaborative signal (solving the challenge C2).

3 LEARNING MODEL: CAM-AE

In this section, we elaborate on the proposed CAM-AE model, comprising an attention-aided AE module and a multi-hop cross-attention module. After showing how to extract and encode multi-hop neighborhood information for a given bipartite graph, we describe implementation details of each module in CAM-AE. We then explain how to optimize our learning model. Finally, we provide analytical findings, which theoretically validate the efficiency of CAM-AE.

3.1 High-Order Connectivity Encoder

To extract multi-hop neighbors of a given user, we may use a bipartite graph constructed by establishing edges based on all user–item interactions. However, using such a bipartite graph will result in a huge memory and computational burden during training. To solve this practical issue, we pre-process the user–item interactions in such a way of initially extracting multi-hop neighbors of a user. This extracted ‘*per-user*’ connectivity information is then made available in the reverse-denoising process to assist recovery of the original user–item interactions (see Figure 2).

Given a target user’s historical interactions \mathbf{u} , we explain how to explore multi-hop neighbors along paths within the user–item bipartite graph. In our study, we encode high-order connectivity information (*i.e.*, high-order collaborative signals) up to H -hop neighbors as in the following form:

$$\mathbf{u}' = [\mathbf{u}^{(2)}, \dots, \mathbf{u}^{(H)}], \quad (5)$$

where

$$\mathbf{u}^{(h)} = \frac{1}{N_{h-1,h}} \mathbf{r}(\mathcal{G}(u, h), \mathbf{c}^{(h)}) \quad (6)$$

for $h = 2, \dots, H$.³ Here, $\mathbf{r}(\cdot, \cdot)$ is the vector-valued function returning a multi-hot encoded vector where one is assigned only to the

³If h is even, then $|\mathbf{u}^{(h)}| = |\mathcal{U}|$. Otherwise, $|\mathbf{u}^{(h)}| = |\mathcal{I}|$. However, to tractably handle \mathbf{u}' , we can set the dimensionality of each $\mathbf{u}^{(h)}$ to $\max\{|\mathcal{U}|, |\mathcal{I}|\}$.

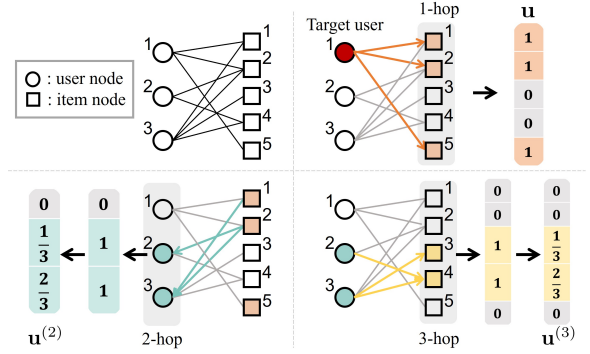


Figure 3: Extraction and encoding of 2-hop and 3-hop neighbors of the target user (*User 1*) as well as direct neighbors for a given bipartite graph.

elements corresponding to h -hop neighbors of user u ; $\mathcal{G}(u, h)$ indicates the set of h -hop neighbors of user u ; $\mathbf{c}^{(h)} \in \mathbb{R}^{|\mathcal{G}(u, h)| \times 1}$ is the integer vector, each of which represents the number of incoming links from $(h-1)$ -hop neighbors of user u to each of h -hop neighbors; and $N_{h-1,h}$ is the total number of interactions between $(h-1)$ -hop and h -hop neighbors of user u . Now, let us show an explicit form of encoded h -hop neighborhood information $\mathbf{u}^{(h)}$ along with the following example.

Example 1. Consider the target user (*User 1*) in the user–item bipartite graph consisting of 3 users and 5 items, as illustrated in Figure 3. Here, it follows that $\mathbf{u} = [1, 1, 0, 0, 1]^T$ as *User 1* has interacted with *Item 1*, *Item 2*, and *Item 5*. Since the 2-hop neighbors of *User 1* are *User 2*, *User 3* and *User 3* has two incoming links, we have $\mathbf{u}^{(2)} = [0, \frac{1}{3}, \frac{2}{3}]^T$ normalized to the total number of interactions at the second hop. Similarly, we obtain $\mathbf{u}^{(3)} = [0, 0, \frac{1}{3}, \frac{2}{3}, 0]^T$.

3.2 Attention-Aided AE Module

VAE-based CF [20] shows great potential in capturing underlying patterns by encoding user–item interactions into a latent space. Similarly, in the CAM-AE model, we would like to design lightweight encoders to project the user–item interactions into a latent space, aiming to capture high-level patterns while keeping the computations manageable by controlling the latent dimension. This design principle enables us to solve the challenge C1.

In CAM-AE, the attention-aided AE module involves *hop-specific* encoders. As illustrated in Figure 2, an encoder $\mathcal{E}_1(\cdot)$ is adopted to project user u ’s noisy interactions \mathbf{u}_t into a latent space, represented by the latent embedding $\mathbf{z}_t \in \mathbb{R}^{k \times 1}$ with its dimensionality k . Likewise, another hop-specific encoder $\mathcal{E}_h(\cdot)$ generates embeddings for the encoded information of h -hop neighbors of user u , $\mathbf{u}^{(h)}$, yielding $\mathbf{z}^{(h)} \in \mathbb{R}^{k \times 1}$. Similarly as in [42], these two encoders $\mathcal{E}_1(\cdot)$ and $\mathcal{E}_h(\cdot)$ are implemented as *linear* transformations, which are formally expressed as

$$\mathbf{z}_t = \mathcal{E}_1(\mathbf{u}_t) = \mathbf{E}_1 \mathbf{u}_t, \quad (7)$$

$$\mathbf{z}^{(h)} = \mathcal{E}_h(\mathbf{u}^{(h)}) = \mathbf{E}_h \mathbf{u}^{(h)}, \quad (8)$$

where $\mathbf{E}_1 \in \mathbb{R}^{k \times |\mathcal{I}|}$ and $\mathbf{E}_h \in \mathbb{R}^{k \times |\mathcal{u}^{(h)}|}$ represents the transformation matrices. Figure 2 illustrates the case where the embeddings $\mathbf{z}^{(2)}$

and $\mathbf{z}^{(3)}$ of both 2-hop and 3-hop neighbors of a target user are generated.⁴ We can preserve the CAM-AE model’s complexity at manageable levels through these linear transformations that reduce the dimension of latent representations.

We turn to addressing a decoder $\mathcal{D}(\cdot)$, which is adopted to recover the mean value of $p_\theta(\mathbf{u}_{t-1} | \mathbf{u}_t, \mathbf{u}')$ using the embedding, denoted as $\bar{\mathbf{z}}_t$, as input that is returned by the multi-hop cross-attention module (to be specified in Section 3.3), as depicted in Figure 2. The decoder is formulated as follows:

$$\hat{\boldsymbol{\mu}}_\theta = \mathcal{D}(\bar{\mathbf{z}}_t) = \mathbf{D}\bar{\mathbf{z}}_t, \quad (9)$$

where $\mathbf{D} \in \mathbb{R}^{|\mathcal{I}| \times k}$ is the transformation matrix in the decoder. Then, \mathbf{u}_{t-1} can be sampled from $p_\theta(\mathbf{u}_{t-1} | \mathbf{u}_t, \mathbf{u}') = \mathcal{N}(\mathbf{u}_{t-1}; \hat{\boldsymbol{\mu}}_\theta, \beta_t \mathbf{I})$.

3.3 Multi-Hop Cross-Attention Module

The CAM-AE model is enlightened by conditional diffusion models [31], which achieved impressive success in various fields by using the cross-attention mechanism [39] to integrate additional conditions. In CAM-AE, high-order connectivity information in Eq. (5) can be regarded as a *condition* for denoising the original user–item interactions \mathbf{u}_0 , following the principle of conditional diffusion models [31]. In this study, to effectively infuse high-order connectivities into our learning model, we propose the multi-hop cross-attention module. This module judiciously harnesses the conditional nature of these connectivities while connecting with the direct user–item interactions in the reverse-denoising process. This design principle is established to fundamentally solve the challenge C2.

In the multi-hop cross-attention module, we start by expanding the dimension of $\mathbf{z}_t \in \mathbb{R}^{k \times 1}$ and $\mathbf{z}^{(h)} \in \mathbb{R}^{k \times 1}$ (i.e., the output embeddings of encoders \mathcal{E}_1 and \mathcal{E}_h) to obtain $\mathbf{v}_t \in \mathbb{R}^{k \times d}$ and $\mathbf{q}^{(h)} \in \mathbb{R}^{k \times d}$ for improving the *expressiveness*. This expansion can be implemented as $\mathbf{v}_t = \mathbf{z}_t \mathbf{E}^v$ and $\mathbf{q}^{(h)} = \mathbf{z}^{(h)} \mathbf{E}^q$, where $\mathbf{E}^v \in \mathbb{R}^{1 \times d}$ and $\mathbf{E}^q \in \mathbb{R}^{1 \times d}$ are the transformation matrices with d being the expanded dimensionality. Then, the resulting embedding of h -hop neighbors of user u , $\mathbf{q}^{(h)}$, is integrated into \mathbf{v}_t using the multi-hop cross-attention module:

$$\text{Attention}_h(\mathbf{Q}^{(h)}, \mathbf{K}_t, \mathbf{V}_t) := \text{softmax}\left(\frac{\mathbf{Q}^{(h)} \mathbf{K}_t^T}{\sqrt{d}}\right) \mathbf{V}_t, \quad (10)$$

where $\mathbf{Q}^{(h)} = \mathbf{q}^{(h)} \mathbf{W}_\theta^Q$, $\mathbf{K}_t = \mathbf{v}_t \mathbf{W}_\theta^K$, and $\mathbf{V}_t = \mathbf{v}_t \mathbf{W}_\theta^V$; and $\text{softmax}(\cdot)$ is the softmax function. Here, $\{\mathbf{W}_\theta^Q, \mathbf{W}_\theta^K, \mathbf{W}_\theta^V\} \in \mathbb{R}^{d \times d}$ are trainable parameters. Figure 2 includes the multi-hop cross-attention module (see the light red blocks in the reverse-denoising process) when 2-hop and 3-hop neighbors of the target user are taken into account.

Due to the fact that the aforementioned process is basically built upon linear transformations that lack the ability to capture the intrinsic data complexity, a per-hop forward operation $f_h(\cdot)$ using *non-linear* transformations is applied to Attention_h [39]. We stack N identical layers, each consisting of cross-attention and non-linear transformation, with the output from the last layer aggregated to

⁴Although the example in Figure 2 deals with up to 3-hop neighbors, it is straightforward to extend our module to the case of leveraging general h -hop neighbors.

form $\bar{\mathbf{z}}_t \in \mathbb{R}^{k \times d}$, calculated as

$$\bar{\mathbf{z}}_t = \sum_{h=2}^H \alpha_h f_h(\text{Attention}_h), \quad (11)$$

where $\sum_{h=2}^H \alpha_h = 1$; α_h is the weight balancing among different $f_h(\cdot)$ ’s specific to hop h ; and H is the number of hops. Finally, $\bar{\mathbf{z}}_t$ is the input of the decoder $\mathcal{D}(\cdot)$ in Eq. (9).

It is worthwhile to note that both \mathbf{v}_t and $\mathbf{q}^{(h)}$ originate from the same user, offering two different perspectives of the same data. This dual perspective is beneficial for precisely capturing the collaborative signal. In other words, through the cross-attention mechanism in CAM-AE, high-order connectivities can significantly improve the reverse-denoising process, thereby ultimately enhancing recommendation accuracies.

3.4 Optimization

In our learning model, the denoising transition $p_\theta(\mathbf{u}_{t-1} | \mathbf{u}_t, \mathbf{u}') = \mathcal{N}(\mathbf{u}_{t-1}; \boldsymbol{\mu}_\theta(\mathbf{u}_t, \mathbf{u}', t), \beta_t \mathbf{I})$ is forced to approximate the tractable distribution $q(\mathbf{u}_{t-1} | \mathbf{u}_t, \mathbf{u}_0) = \mathcal{N}(\mathbf{u}_{t-1}; \tilde{\boldsymbol{\mu}}(\mathbf{u}_t, \mathbf{u}_0), \beta_t \mathbf{I})$ (note that the mean $\tilde{\boldsymbol{\mu}}(\mathbf{u}_t, \mathbf{u}_0)$ can be computed via Bayes’ rule as shown in [15]: $q(\mathbf{u}_{t-1} | \mathbf{u}_t, \mathbf{u}_0) = q(\mathbf{u}_t | \mathbf{u}_{t-1}, \mathbf{u}_0) \frac{q(\mathbf{u}_{t-1} | \mathbf{u}_0)}{q(\mathbf{u}_t | \mathbf{u}_0)}$). Following this approximation, we can generate \mathbf{u}_{t-1} from \mathbf{u}_t progressively until \mathbf{u}_0 is reconstructed. Figure 2 visualizes a single denoising step from \mathbf{u}_T to \mathbf{u}_{T-1} , which is repeated T times to obtain \mathbf{u}_0 .

To optimize the parameter θ , our model aims at minimizing the variational lower bound (VLB) [15, 18] for the observed user–item interactions \mathbf{u}_0 alongside the following loss:

$$\mathcal{L}_{\text{VLB}} = \mathcal{L}_0 + \sum_{t=2}^T \mathcal{L}_{t-1}, \quad (12)$$

where $\mathcal{L}_0 = \mathbb{E}_q[-\log p_\theta(\mathbf{u}_0 | \mathbf{u}_1, \mathbf{u}')] is the reconstruction term to recover the original interactions \mathbf{u}_0 ; and \mathcal{L}_{t-1} is the denoising matching term, regulating $p_\theta(\mathbf{u}_{t-1} | \mathbf{u}_t, \mathbf{u}')$ to align with the tractable distribution $q(\mathbf{u}_{t-1} | \mathbf{u}_t, \mathbf{u}_0)$, served as the ground truth, and is given by$

$$\begin{aligned} \mathcal{L}_{t-1} &= \mathbb{E}_q [D_{\text{KL}}(q(\mathbf{u}_{t-1} | \mathbf{u}_t, \mathbf{u}_0) \| p_\theta(\mathbf{u}_{t-1} | \mathbf{u}_t, \mathbf{u}'))] \\ &= \mathbb{E}_q \left[\frac{1}{2\beta_t} [\|\boldsymbol{\mu}_\theta(\mathbf{u}_t, \mathbf{u}', t) - \tilde{\boldsymbol{\mu}}(\mathbf{u}_t, \mathbf{u}_0)\|^2] \right], \end{aligned} \quad (13)$$

where $D_{\text{KL}}(\cdot \| \cdot)$ denotes the Kullback–Leibler (KL) divergence between two distributions.

3.5 Theoretical Analyses

In this subsection, we are interested in theoretically showing the efficiency of the CAM-AE model. In CAM-AE, we use an AE to generate embeddings, reducing computations to an acceptable level by controlling the embedding dimension k . We first establish the following theorem, which analyzes that the potential difference incurred by using our low-complexity modules in CAM-AE is negligibly small compared to the (computationally more expensive) original cross-attention [39], defined as

$$\text{Attention}(\mathbf{Q}, \mathbf{K}, \mathbf{V}) := \text{softmax}\left(\frac{\mathbf{Q} \mathbf{K}^T}{\sqrt{d}}\right) \mathbf{V}, \quad (14)$$

where $\mathbf{Q} = \mathbf{q}\tilde{\mathbf{W}}_{\theta}^{\mathbf{Q}}$, $\mathbf{K} = \mathbf{k}\tilde{\mathbf{W}}_{\theta}^{\mathbf{K}}$, and $\mathbf{V} = \mathbf{v}\tilde{\mathbf{W}}_{\theta}^{\mathbf{V}}$. Here, $\mathbf{q} \in \mathbb{R}^{\max\{|\mathcal{U}|, |\mathcal{I}|\} \times d}$ and $\{\mathbf{k}, \mathbf{v}\} \in \mathbb{R}^{|\mathcal{I}| \times d}$ are the embedding matrices and $\{\tilde{\mathbf{W}}_{\theta}^{\mathbf{Q}}, \tilde{\mathbf{W}}_{\theta}^{\mathbf{K}}, \tilde{\mathbf{W}}_{\theta}^{\mathbf{V}}\} \in \mathbb{R}^{d \times d}$ are trainable parameters of *Attention* in Eq. (14).

THEOREM 1. *Suppose that $\max\{|\mathcal{U}|, |\mathcal{I}|\}$ is sufficiently large. If $k \geq 5\ln(\max\{|\mathcal{U}|, |\mathcal{I}|\})/(\varepsilon^2 - \varepsilon^3)$, then there exist matrices $\mathbf{E}_{\mathbf{Q}} \in \mathbb{R}^{k \times \max\{|\mathcal{U}|, |\mathcal{I}|\}}$, $\mathbf{E}_{\mathbf{K}}, \mathbf{E}_{\mathbf{V}} \in \mathbb{R}^{k \times |\mathcal{I}|}$ and $\mathbf{D} \in \mathbb{R}^{|\mathcal{I}| \times k}$ such that*

$$\Pr\left(\left|\frac{\left\|\mathbf{D} \cdot \text{softmax}\left(\mathbf{E}_{\mathbf{Q}}\mathbf{A}\mathbf{E}_{\mathbf{K}}^T\right)\mathbf{E}_{\mathbf{V}}\mathbf{V}\right\|}{\text{softmax}(\mathbf{A})\mathbf{V}} - 1\right| \leq \varepsilon\right) > 1 - o(1), \quad (15)$$

where $\mathbf{Q} \in \mathbb{R}^{\max\{|\mathcal{U}|, |\mathcal{I}|\} \times d}$ and $\{\mathbf{K}, \mathbf{V}\} \in \mathbb{R}^{|\mathcal{I}| \times d}$ are the embedding matrices in the original cross-attention; $\mathbf{A} = \frac{\mathbf{Q}\mathbf{K}^T}{\sqrt{d}}$; and $\varepsilon > 0$ is an arbitrarily small constant.

The proof of Theorem 1 is omitted due to page limitations. Theorem 1 implies that the probability that the two terms $\text{softmax}(\mathbf{A})\mathbf{V}$ and $\mathbf{D} \cdot \text{softmax}\left(\mathbf{E}_{\mathbf{Q}}\mathbf{A}\mathbf{E}_{\mathbf{K}}^T\right)\mathbf{E}_{\mathbf{V}}\mathbf{V}$ are approximately equal approaches one asymptotically when the maximum value of $|\mathcal{U}|$ and $|\mathcal{I}|$ is sufficiently large. We are capable of bridging this theorem and our CAM-AE model by setting $\mathbf{E}_{\mathbf{V}}\mathbf{V} = \mathbf{V}_t$, $\mathbf{E}_{\mathbf{K}}\mathbf{K} = \mathbf{K}_t$, $\mathbf{E}_{\mathbf{Q}}\mathbf{Q} = \mathbf{Q}^{(h)}$, and \mathbf{D} as in Eq. (9), where $\mathbf{E}_{\mathbf{Q}} = \mathbf{E}_h$, $\mathbf{E}_{\mathbf{K}} = \mathbf{E}_1$, and $\mathbf{E}_{\mathbf{V}} = \mathbf{E}_1$, which leads to the conclusion that the term $\mathbf{D} \cdot \text{softmax}\left(\mathbf{E}_{\mathbf{Q}}\mathbf{A}\mathbf{E}_{\mathbf{K}}^T\right)\mathbf{E}_{\mathbf{V}}\mathbf{V}$ in Eq. (15) is equivalent to $\mathbf{D} \cdot \text{Attention}_h\left(\mathbf{Q}^{(h)}, \mathbf{K}_t, \mathbf{V}_t\right)$. From Theorem 1, one can see that the original cross-attention can be effectively approximated by our low-complexity modules in CAM-AE, which combines the cross-attention mechanism with *linear* transformations, thus significantly reducing the computational complexity (which is to be empirically validated later). In other words, we can control k to maintain the amount of computations manageable while ensuring that the embeddings generated by our model closely approximate those from the original cross-attention, especially for large $\max\{|\mathcal{U}|, |\mathcal{I}|\}$.

Additionally, to validate the scalability of the CAM-AE model, we analytically show its computational complexity during training by establishing the following theorem.

THEOREM 2. *The computational complexity of CF-Diff training, including both the computation time of the forward-diffusion process and the training time of the reverse-denoising process, is given by $\mathcal{O}(\max\{|\mathcal{U}|, |\mathcal{I}|\})$.*

The proof of Theorem 2 is omitted due to page limitations. From Theorem 2, one can see that the computational complexity required to train CF-Diff scales *linearly* with the maximum between the number of users and the number of items. This is because we are capable of considerably reducing the computation of Eq. (10) (corresponding to the cross-attention part in Figure 2) by controlling the embedding dimension k .

4 EXPERIMENTAL EVALUATION

In this section, we systematically conduct extensive experiments to answer the following five key research questions (RQs):

- **RQ1:** How much does CF-Diff improve the top- K recommendation over benchmark recommendation methods?

Table 1: The statistics of three datasets.

Dataset	# of users	# of items	# of interactions
MovieLens-1M	5,949	2,810	571,531
Yelp	54,574	34,395	1,402,736
Anime	73,515	11,200	7,813,737

- **RQ2:** How does each component in CAM-AE contribute to the recommendation accuracy?
- **RQ3:** How many hops in CF-Diff benefit for the recommendation accuracy?
- **RQ4:** How do key parameters of CAM-AE affect the performance of CF-Diff?
- **RQ5:** How scalable is CF-Diff when the size of datasets increases?

4.1 Experimental Settings

Datasets. We conduct our experiments on three real-world datasets widely adopted for evaluating the performance of recommender systems, which include MovieLens-1M (ML-1M)⁵, and two larger datasets, Yelp⁶ and Anime⁷. Table 1 provides a summary of the statistics for each dataset.

Competitors To comprehensively demonstrate the superiority of CF-Diff, we present nine recommendation methods, including five general benchmark CF methods (NGCF [44], LightGCN [13], SGL [45], NCL [23], and BSPM [8]) and four generative model-based recommendation methods (CFGAN [6], MultiDAE [47], RecVAE [35], and DiffRec [43]).

Performance metrics. We follow the full-ranking protocol [13] by ranking all the non-interacted items for each user. In our study, we adopt two widely used ranking metrics, Recall@ K (R@ K) and NDCG@ K (N@ K), where $K \in \{10, 20\}$.

Implementation details. We use the best hyperparameters of competitors and CF-Diff obtained by extensive hyperparameter tuning on the validation set. We use the Adam optimizer [17], where the batch size is selected in the range of $\{32, 64, 128, 256\}$. In CF-Diff, the hyperparameters used in the diffusion model (e.g., the noise scale β_t and the diffusion step T) essentially follow the settings in [43]. We choose the best hyperparameters in the following ranges: $\{1, 2, 3, 4\}$ for the number of hops, H ; $\{512, 1024, 2048\}$ for the latent dimension k in the attention-aided AE module; and $\{16, 32, 64, 128\}$ for the expanded dimension d , $\{1, 2, 3, 4\}$ for the number of layers, N , and $\{0.3, 0.5, 0.7\}$ for α_h 's in the multi-hop cross-attention module. All experiments are carried out with Intel (R) 12-Core (TM) E5-1650 v4 CPUs @ 3.60 GHz and GPU of NVIDIA GeForce RTX 3080. The code of CF-Diff is available at https://github.com/jackfrost168/CF_Diff.

4.2 Results and Analyses

In RQ1–RQ3, we provide experimental results on all datasets. For RQ4, we show here only the results on ML-1M in terms of N@ K due to space limitations, since the results on other datasets and metrics showed similar tendencies to those on ML-1M. Additionally, we highlight the best and second-best performers in each case of the following tables in bold and underline, respectively.

⁵<https://grouplens.org/datasets/movielens/1m/>.

⁶<https://www.yelp.com/dataset/>.

⁷<https://www.kaggle.com/datasets/CooperUnion/anime-recommendations-database>.

Table 2: Performance comparison among CF-Diff and nine recommendation competitors for the three benchmark datasets. Here, the best and second-best performers are highlighted by bold and underline, respectively.

Method	ML-1M				Yelp				Anime			
	R@10	R@20	N@10	N@20	R@10	R@20	N@10	N@20	R@10	R@20	N@10	N@20
NGCF	0.0864	0.1484	0.0805	0.1008	0.0428	0.0726	0.0255	0.0345	0.1924	0.2888	0.3515	0.3485
LightGCN	0.0824	0.1419	0.0793	0.0982	0.0505	0.0858	0.0312	0.0417	0.2071	0.3043	0.3937	0.3824
SGL	0.0806	0.1355	0.0799	0.0968	0.0564	<u>0.0944</u>	0.0346	0.0462	0.1994	0.2918	0.3748	0.3652
NCL	0.0878	0.1471	0.0819	0.1011	0.0535	0.0906	0.0326	0.0438	0.2063	0.3047	0.3915	0.3819
BSPM	0.0884	0.1494	0.0750	0.0957	<u>0.0565</u>	0.0932	0.0331	0.0439	0.2054	<u>0.3103</u>	0.4355	0.4231
CFGAN	0.0684	0.1181	0.0663	0.0828	0.0206	0.0347	0.0129	0.0172	0.1946	0.2889	0.4601	0.4289
MultiDAE	0.0769	0.1335	0.0737	0.0919	0.0531	0.0876	0.0316	0.0421	0.2142	0.3085	0.4177	0.4125
RecVAE	0.0835	0.1422	0.0769	0.0963	0.0493	0.0824	0.0303	0.0403	0.2137	0.3068	0.4105	0.4068
DiffRec	<u>0.1021</u>	<u>0.1763</u>	<u>0.0877</u>	<u>0.1131</u>	0.0554	0.0914	<u>0.0343</u>	<u>0.0452</u>	<u>0.2104</u>	0.3012	<u>0.5047</u>	<u>0.4649</u>
CF-Diff	0.1077	0.1843	0.0912	0.1176	0.0585	0.0962	0.0368	0.0480	0.2191	0.3155	0.5152	0.4748

4.2.1 *Comparison with nine recommendation competitors (RQ1).* We validate the superiority of CF-Diff over nine recommendation competitors through extensive experiments on the three datasets. Table 2 summarizes the results, and we make the following insightful observations.

- (1) Our CF-Diff *consistently* and *significantly* outperforms all recommendation competitors regardless of the datasets and the performance metrics.
- (2) The second-best performer tends to be DiffRec. Its superior performance among other generative model-based methods can be attributed to the use of diffusion models, known for their state-of-the-art performance in various fields. This enables DiffRec to more intricately recover user-item interactions for recommendations compared to VAE-based CF methods. However, DiffRec is consistently inferior to CF-Diff, primarily because it overlooks the high-order connectivity information, which is essential for capturing crucial collaborative signals.
- (3) The performance gap between CF-Diff (X) and Diffrec (Y) is the largest when the Yelp dataset is used; the maximum improvement rate of 7.29% is achieved in terms of $N@10$, where the improvement rate (%) is given by $\frac{X-Y}{Y} \times 100$.
- (4) Compared with GNN-based methods (NGCF, LightGCN, SGL, and NCL) that exploit high-order connectivity information through the message passing mechanism, our CF-Diff method exhibits remarkable gains. This superiority basically stems from the ability of inherently powerful diffusion models and avoiding the over-smoothing issue when integrating high-order connectivities.
- (5) CFGAN shows relatively lower accuracies compared to other generative model-based methods. This performance degradation is caused by mode collapse during GAN training, resulting in inferior recommendation outcomes.

4.2.2 *Impact of components in CAM-AE (RQ2).* To discover what role each component plays in the success of our learning model, CAM-AE, we conduct an ablation study by removing or replacing each component in CAM-AE.

- CAM-AE: corresponds to the original CAM-AE model.
- CAM-AE-att: removes the multi-hop cross-attention module in CAM-AE.

Table 3: Performance comparison among CAM-AE and its three variants. Here, the best and second-best performers are highlighted by bold and underline, respectively.

Dataset	Method	R@10	R@20	N@10	N@20
ML-1M	CAM-AE-att	0.1016	0.1751	0.0873	0.1123
	CAM-AE-ae	0.1024	0.1732	0.0871	0.1117
	CAM-AE-self	<u>0.1057</u>	<u>0.1794</u>	<u>0.0891</u>	<u>0.1144</u>
	CAM-AE	0.1077	0.1843	0.0912	0.1176
Yelp	CAM-AE-att	0.0553	0.0905	0.0342	0.0448
	CAM-AE-ae	OOM	OOM	OOM	OOM
	CAM-AE-self	<u>0.0574</u>	<u>0.0952</u>	<u>0.0355</u>	<u>0.0469</u>
	CAM-AE	0.0585	0.0962	0.0368	0.0480
Anime	CAM-AE-att	0.2091	0.3024	0.5023	0.4623
	CAM-AE-ae	OOM	OOM	OOM	OOM
	CAM-AE-self	<u>0.2112</u>	<u>0.3094</u>	<u>0.5079</u>	<u>0.4678</u>
	CAM-AE	0.2191	0.3155	0.5152	0.4748

- CAM-AE-ae: removes the attention-aided AE in CAM-AE.
- CAM-AE-self: replaces the multi-hop cross-attention module in CAM-AE with the multi-hop *self-attention* module, which ignores the high-order connectivity information (by replacing $q^{(h)}$ with v_t).

The performance comparison among the original CAM-AE and its three variants is presented in Table 3 with respect to $R@K$ and $N@K$ on the three datasets. Our findings are as follows:

- (1) The original CAM-AE always exhibits substantial gains over the other variants, which demonstrates that each component in CAM-AE plays a crucial role in enhancing the recommendation accuracy.
- (2) CAM-AE outperforms CAM-AE-att, which can be attributed to the fact that the multi-hop cross-attention module is capable of infusing high-order connectivities into the proposed method to improve the performance of recommendations via CF.
- (3) The performance gain of CAM-AE over CAM-AE-ae is relatively higher than that of the other variants for the ML-1M dataset. Additionally, the attention-aided AE’s removal leads to out-of-memory (OOM) issues on the Yelp and Anime datasets, signifying its crucial role not only in extracting representations that can precisely capture the underlying

Table 4: Performance comparison according to different values of H . Here, the best and second-best performers are highlighted by bold and underline, respectively.

Dataset	Method	R@10	R@20	N@10	N@20
ML-1M	CF-Diff-2	<u>0.1062</u>	<u>0.1786</u>	<u>0.0907</u>	<u>0.1164</u>
	CF-Diff-3	0.1077	0.1843	0.0912	0.1176
	CF-Diff-4	0.1055	0.1764	0.0883	0.1134
Yelp	CF-Diff-2	<u>0.0572</u>	<u>0.0935</u>	<u>0.0351</u>	<u>0.0462</u>
	CF-Diff-3	0.0585	0.0962	0.0368	0.0480
	CF-Diff-4	0.0561	0.0917	0.0347	0.0455
Anime	CF-Diff-2	0.2191	0.3155	0.5152	0.4748
	CF-Diff-3	<u>0.2082</u>	<u>0.3021</u>	<u>0.4998</u>	<u>0.4586</u>
	CF-Diff-4	0.1938	0.2824	0.4605	0.4236

patterns of user–item interactions but also in maintaining the computational complexity at acceptable levels.

- (4) CAM-AE is superior to CAM-AE-self. This confirms that infusing high-order connectivity information enriches the collaborative signal and thus results in performance enhancement even under a diffusion-model framework.

4.2.3 The impact of multi-hop neighbors (RQ3). To investigate how many hop neighbors in the CF-Diff method are informative, we present a variant of CF-Diff, CF-Diff- H , which considers up to H -hop neighbors *constantly* instead of optimally searching for the value of H depending on a given dataset. The results are shown in Table 4 and our observations are as follows:

- (1) CF-Diff-3 outperforms CF-Diff-2 on ML-1M and Yelp, indicating that incorporating a wider range of neighboring nodes into the CAM-AE model can positively influence the recommendation results through CF.
- (2) CF-Diff-2 shows the highest recommendation accuracy on Anime. This means that 2-hop neighbors sufficiently capture the collaborative signal, and there is no need for exploiting higher-order connectivity information in this dataset.
- (3) Notably, there is a decline in the performance of CF-Diff-4, because infusing 4-hop neighbors introduces an excess of global connectivity information. This surplus information potentially acts as noise, thereby interfering the personalized recommendations.

4.2.4 The effect of hyperparameters (RQ4). We analyze the impact of key parameters of CAM-AE, including k , d , N , and α_h , on the recommendation accuracy for the ML-1M dataset. In this experiment, we consider 3-hop neighbors (*i.e.*, $H = 3$). For notational convenience, we denote $\alpha_2 = \alpha$ and $\alpha_3 = 1 - \alpha$, which signify the importance of 2-hop and 3-hop neighbors, respectively. When a hyperparameter varies so that its effect is clearly revealed, other parameters are set to the following pivot values: $k = 500$, $d = 16$, $N = 2$, $\alpha = 0.7$. Our findings are as follows:

(Effect of k) From Figure 4a, the maximum N@10 and N@20 are achieved at $k = 500$ on ML-1M. It reveals that high values of k degrade the performance since the resulting embeddings contain more noise and low values of k result in insufficient information during training. Hence, it is crucial to suitably determine the value of k in guaranteeing satisfactory performance.

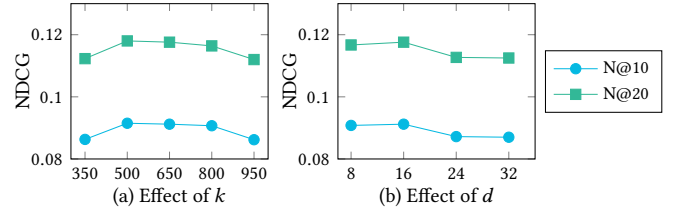


Figure 4: The effect of hyperparameters k and d on N@K for the ML-1M dataset.

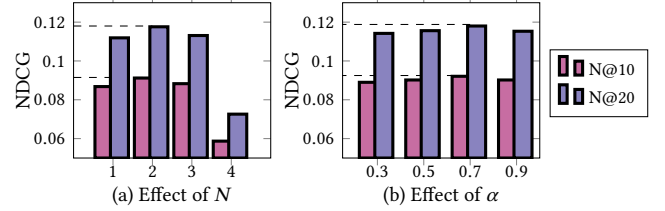


Figure 5: The effect of hyperparameters N and α on N@K for the ML-1M dataset.

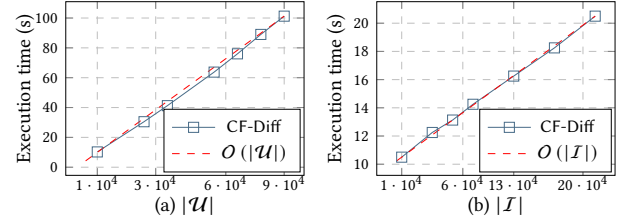


Figure 6: The computational complexity of CF-Diff, where the plots of the execution time versus $|\mathcal{U}|$ in Figure 6a and the execution time versus $|\mathcal{I}|$ in Figure 6b are shown.

(Effect of d) From Figure 4b, the maximum N@10 and N@20 are achieved at $d = 16$ on ML-1M. Using values of d that are too high and too low has a negative impact on the model’s expressiveness. Thus, it is important to appropriately determine the value of d depending on the datasets.

(Effect of N) From Figure 5a, the maximum N@10 and N@20 are achieved at $N = 2$ on ML-1M. A higher N rather degrades the performance, possibly due to the over-fitting problem. Thus, the value of N should be carefully chosen based on given datasets.

(Effect of α) Figure 5b shows that the maximum N@10 and N@20 are achieved at $\alpha = 0.7$ on ML-1M. Tuning α is crucial since it directly determines the model’s ability while balancing between neighbors that are different hops away from the target user, which in turn affects the recommendation performance.

4.2.5 Computational complexity (RQ5). To empirically validate the scalability of our CF-Diff method, we measure the execution time during training on synthetic datasets having user–item interactions. These interactions are generated purely at random, simulating a sparsity level of 0.99, analogous to that observed on Yelp and Anime. By setting different $|\mathcal{U}|$ ’s and $|\mathcal{I}|$ ’s, we can create user–item interactions of various sizes. More specifically, we generate two sets of user–item interactions: in the first set, we generate a set of interactions with $|\mathcal{I}| = 1e^4$ and $|\mathcal{U}| = \{1e^4, 3e^4, 4e^4, 6e^4, 7e^4, 8e^4, 9e^4\}$; and in the second set, we generate another set of interactions with $|\mathcal{U}| = 1e^4$ and $|\mathcal{I}| = \{1e^4, 4e^4, 6e^4, 8e^4, 12e^4, 16e^4, 20e^4\}$. Figure 6a

(*resp.* Figure 6b) illustrates the execution time (in seconds) per iteration of CF-Diff, including the forward-diffusion process and the reverse-denoising process, as the number of users (*resp.* the number of items) increases. The dashed line indicates a linear scaling in $|\mathcal{U}|$ and $|\mathcal{I}|$, derived from Theorem 2. It can be seen that our empirical evaluation concurs with the theoretical analysis.

5 RELATED WORK

In this section, we review some representative methods in two broad fields of research, including 1) benchmark CF methods and 2) generative model-based recommendation methods.

5.1 General Benchmark CF

The most common paradigm of CF is to factorize the user–item interaction matrix into lower-dimensional matrices [19, 28, 30]. The dot product in MF can be replaced with a multi-layer perceptron (MLP) to capture the non-linearities in the complex behavior of such interactions [7, 14]. To analyze beyond direct user connections to items, high-order connectivities are essential for understanding the user preferences, leading to the rise of GNNs in CF for modeling these complex relationships [4]. GC-MC [4] first proposed a graph AE framework for recommendations using message passing on the user–item bipartite graph. NGCF [44] employed GNNs to propagate user and item embeddings on the bipartite graph capturing the collaborative signal in complex high-order connectivities. NIA-GCN [38] was developed by taking into account both the relational information between neighboring nodes and the heterogeneous nature of the user–item bipartite graph. LightGCN [13] improved the performance by lightweight message passing, omitting feature transformation and nonlinear activation. UltraGCN [26] advanced efficiency by skipping infinite layers of explicit message passing and directly approximating graph convolution limits with a constraint loss. BSPM [8] made a connection between the concept of blurring-sharpening process models and graph filtering [34], utilizing ordinary differential equations to model the perturbation and recovery of user–item interactions. Additionally, contrastive learning was used to further improve the recommendation accuracy by taking node self-discrimination into account [23, 45].

5.2 Generative Model-Based Recommendation

GAN-based methods. Generative adversarial network (GAN)-based models in CF employ a generator to estimate user–item interaction probabilities, optimized through adversarial training [11, 12, 41, 46]. RecGAN [5] combined recurrent neural network (RNN) with GAN for capturing complex user–item interaction patterns, while CFGAN [6] enhanced the recommendation accuracy with real-valued vector-wise adversarial learning. Nevertheless, adversarial training is often associated with training instability and mode collapse, potentially leading to suboptimal performance [1, 27].

VAE-based methods. The denoising AE (DAE) was firstly used for top- K recommendations, learning latent representations from corrupted user preferences [47]. CVAE [20] extended this by using a VAE to learn latent representations of items from ratings and multimedia content for multimedia recommendations. A series of VAE-based methods [22, 25, 35] were further developed for CF with

implicit feedback, enhancing the accuracy, interpretability, and robustness by incorporating a multinomial likelihood and a Bayesian approach for user preference modeling. However, VAE-based models struggle to balance between simplicity and representations of complex data, with simpler models possibly failing to capture diverse user preferences and more complex models potentially being computationally intractable [36].

Diffusion model-based methods. Recently, diffusion models have achieved state-of-the-art performance in image generation by decomposing the image generation process into a series of DAEs. CODIGEM [40] extended this with the denoising diffusion probabilistic model (DDPM) in [15] to recommender systems, leveraging the intricate and non-linear patterns in the user–item interaction matrix. Additionally, diffusion models have been successfully applied to sequential recommendations [21, 24, 48, 50]. Inspired by score-based generative models [37], DiffRec [43] accommodated diffusion models to predict unknown user–item interactions in a denoising manner by gradually corrupting interaction histories with scheduled Gaussian noise and then recovering the original interactions iteratively through a neural network.

Discussion. Despite the impressive performance of current diffusion model-based recommender systems, existing models overlook high-order user–item connectivities that reveal co-preference patterns between users and items. These high-order connectivities among users and items are crucial in CF performed with limited direct user–item interactions, aiding in delivering more precise and personalized recommendations. However, effectively incorporating such high-order connectivity information remains a significant challenge in diffusion model-based CF.

6 CONCLUSIONS

In this paper, we explored an open yet fundamental problem of how to empower CF-based recommender systems when diffusion models are employed as a core framework for training. To tackle this challenge, we proposed CF-Diff, a diffusion model-based approach for generative recommender systems, designed to infuse high-order connectivity information into our own learning model, CAM-AE, while preserving the model’s complexity at manageable levels. Through extensive experiments on three real-world benchmark datasets, we demonstrated (a) the superiority of CF-Diff over nine state-of-the-art recommendation methods while showing dramatic gains up to 7.29% in terms of NDCG@10 compared to the best competitor, (b) the theoretical findings that analytically confirm the computational tractability and scalability of CF-Diff, (c) the effectiveness of core components in CAM-AE, and (d) the impact of tuning key hyperparameters in CAM-AE.

ACKNOWLEDGMENTS

This work was supported by the National Research Foundation of Korea (NRF), Republic of Korea Grant by the Korean Government through MSIT under Grants 2021R1A2C3004345 and RS-2023-00220762 and by the Institute of Information and Communications Technology Planning and Evaluation (IITP), Republic of Korea Grant by the Korean Government through MSIT (6G Post-MAC-Positioning and Spectrum-Aware intelligent MAC for Computing and Communication Convergence) under Grant 2021-0-00347.

REFERENCES

- [1] Martin Arjovsky and Léon Bottou. 2017. Towards principled methods for training generative adversarial networks. In *ICLR*.
- [2] Jacob Austin, Daniel D Johnson, Jonathan Ho, Daniel Tarlow, and Rianne Van Den Berg. 2021. Structured denoising diffusion models in discrete state-spaces. In *NeurIPS*. 17981–17993.
- [3] Omri Avrahami, Dani Lischinski, and Ohad Fried. 2022. Blended diffusion for text-driven editing of natural images. In *CVPR*. 18208–18218.
- [4] Rianne van den Berg, Thomas N Kipf, and Max Welling. 2018. Graph convolutional matrix completion. In *KDD (Deep Learning Day)*.
- [5] Homanga Bharadhwaj, Homin Park, and Brian Y Lim. 2018. RecGAN: Recurrent generative adversarial networks for recommendation systems. In *RecSys*. 372–376.
- [6] Dong-Kyu Chae, Jin-Soo Kang, Sang-Wook Kim, and Jung-Tae Lee. 2018. CFGAN: A generic collaborative filtering framework based on generative adversarial networks. In *CIKM*. 137–146.
- [7] Chong Chen, Min Zhang, Yongfeng Zhang, Yiqun Liu, and Shaoping Ma. 2020. Efficient neural matrix factorization without sampling for recommendation. *ACM Transactions on Information Systems (TOIS)* 38, 2 (2020), 1–28.
- [8] Jeongwhan Choi, Seoyoung Hong, Noseong Park, and Sung-Bae Cho. 2023. Blurring-sharpening process models for collaborative filtering. In *SIGIR*. 1096–1106.
- [9] Kamil Deja, Anna Kuzina, Tomasz Trzcinski, and Jakub Tomczak. 2022. On analyzing generative and denoising capabilities of diffusion-based deep generative models. In *NeurIPS*. 26218–26229.
- [10] Prafulla Dhariwal and Alexander Nichol. 2021. Diffusion models beat gans on image synthesis. In *NeurIPS*. 8780–8794.
- [11] Ian Goodfellow, Jean Pouget-Abadie, Mehdi Mirza, Bing Xu, David Warde-Farley, Sherjil Ozair, Aaron Courville, and Yoshua Bengio. 2014. Generative adversarial nets. In *NeurIPS*. 2672–2680.
- [12] Guibing Guo, Huan Zhou, Bowei Chen, Zhirong Liu, Xiao Xu, Xu Chen, Zhenhua Dong, and Xiuqiang He. 2020. IPGAN: Generating informative item pairs by adversarial sampling. *IEEE Transactions on Neural Networks and Learning Systems* 33, 2 (2020), 694–706.
- [13] Xiangnan He, Kuan Deng, Xiang Wang, Yan Li, Yongdong Zhang, and Meng Wang. 2020. LightGCN: Simplifying and powering graph convolution network for recommendation. In *SIGIR*. 639–648.
- [14] Xiangnan He, Lizi Liao, Hanwang Zhang, Liqiang Nie, Xia Hu, and Tat-Seng Chua. 2017. Neural collaborative filtering. In *WWW*. 173–182.
- [15] Jonathan Ho, Ajay Jain, and Pieter Abbeel. 2020. Denoising diffusion probabilistic models. In *NeurIPS*. 6840–6851.
- [16] Chin-Wei Huang, Jae Hyun Lim, and Aaron C Courville. 2021. A variational perspective on diffusion-based generative models and score matching. In *NeurIPS*. 22863–22876.
- [17] Diederik P Kingma and Jimmy Ba. 2015. Adam: A method for stochastic optimization. In *ICLR (Poster)*.
- [18] Diederik P Kingma and Max Welling. 2014. Auto-encoding variational bayes. In *ICLR*.
- [19] Yehuda Koren, Robert Bell, and Chris Volinsky. 2009. Matrix factorization techniques for recommender systems. *Computer* 42, 8 (2009), 30–37.
- [20] Xiaopeng Li and James She. 2017. Collaborative variational autoencoder for recommender systems. In *KDD*. 305–314.
- [21] Zihao Li, Aixin Sun, and Chenliang Li. 2023. DiffuRec: A diffusion model for sequential recommendation. *ACM Transactions on Information Systems* 42, 3 (2023), 1–28.
- [22] Dawen Liang, Rahul G Krishnan, Matthew D Hoffman, and Tony Jebara. 2018. Variational autoencoders for collaborative filtering. In *WWW*. 689–698.
- [23] Zihan Lin, Changxin Tian, Yupeng Hou, and Wayne Xin Zhao. 2022. Improving graph collaborative filtering with neighborhood-enriched contrastive learning. In *WWW*. 2320–2329.
- [24] Qidong Liu, Fan Yan, Xiangyu Zhao, Zhaocheng Du, Huifeng Guo, Ruiming Tang, and Feng Tian. 2023. Diffusion augmentation for sequential recommendation. In *CIKM*. 1576–1586.
- [25] Jianxin Ma, Chang Zhou, Peng Cui, Hongxia Yang, and Wenwu Zhu. 2019. Learning disentangled representations for recommendation. In *NeurIPS*. 5712–5723.
- [26] Kelong Mao, Jieming Zhu, Xi Xiao, Biao Lu, Zhaowei Wang, and Xiuqiang He. 2021. UltraGCN: Ultra simplification of graph convolutional networks for recommendation. In *CIKM*. 1253–1262.
- [27] Luke Metz, Ben Poole, David Pfau, and Jascha Sohl-Dickstein. 2017. Unrolled generative adversarial networks. In *ICLR (Poster)*.
- [28] Andriy Mnih and Russ R Salakhutdinov. 2007. Probabilistic matrix factorization. In *NeurIPS*. 1257–1264.
- [29] Jin-Duk Park, Siqing Li, Xin Cao, and Won-Yong Shin. 2023. Criteria tell you more than ratings: Criteria preference-aware light graph convolution for effective multi-criteria recommendation. In *KDD*. 1808–1819.
- [30] Steffen Rendle, Christoph Freudenthaler, Zeno Gantner, and Lars Schmidt-Thieme. 2009. BPR: Bayesian personalized ranking from implicit feedback. In *UAI*. 452–461.
- [31] Robin Rombach, Andreas Blattmann, Dominik Lorenz, Patrick Esser, and Björn Ommer. 2022. High-resolution image synthesis with latent diffusion models. In *CVPR*. 10684–10695.
- [32] Chitwan Saharia, William Chan, and et al. 2022. Photorealistic text-to-image diffusion models with deep language understanding. In *NeurIPS*. 36479–36494.
- [33] Nikolay Savinov, Junyoung Chung, Mikolaj Binkowski, Erich Elsen, and Aaron van den Oord. 2022. Step-unrolled denoising autoencoders for text generation. In *ICLR*.
- [34] Yifei Shen, Yongji Wu, Yao Zhang, Caihua Shan, Jun Zhang, B Khaled Letaief, and Dongsheng Li. 2021. How powerful is graph convolution for recommendation?. In *CIKM*. 1619–1629.
- [35] Ilya Shenbin, Anton Alekseev, Elena Tutubalina, Valentin Malykh, and Sergey I Nikolenko. 2020. RecVAE: A new variational autoencoder for top-N recommendations with implicit feedback. In *WSDM*. 528–536.
- [36] Jascha Sohl-Dickstein, Eric Weiss, Niru Maheswaranathan, and Surya Ganguli. 2015. Deep unsupervised learning using nonequilibrium thermodynamics. In *ICML*. 2256–2265.
- [37] Yang Song, Jascha Sohl-Dickstein, Diederik P Kingma, Abhishek Kumar, Stefano Ermon, and Ben Poole. 2020. Score-based generative modeling through stochastic differential equations. In *ICLR*.
- [38] Jianing Sun, Yingxue Zhang, Wei Guo, Huifeng Guo, Ruiming Tang, Xiuqiang He, Chen Ma, and Mark Coates. 2020. Neighbor interaction aware graph convolution networks for recommendation. In *SIGIR*. 1289–1298.
- [39] Ashish Vaswani, Noam Shazeer, Niki Parmar, Jakob Uszkoreit, Llion Jones, Aidan N Gomez, Lukasz Kaiser, and Illia Polosukhin. 2017. Attention is all you need. In *NeurIPS*. 6000–6010.
- [40] Joojo Walker, Ting Zhong, Fengli Zhang, Qiang Gao, and Fan Zhou. 2022. Recommendation via collaborative diffusion generative model. In *KSEM*. Springer, 593–605.
- [41] Jun Wang, Lantao Yu, Weinan Zhang, Yu Gong, Yinghui Xu, Benyou Wang, Peng Zhang, and Dell Zhang. 2017. IRGAN: A minimax game for unifying generative and discriminative information retrieval models. In *SIGIR*. 515–524.
- [42] Sinong Wang, Belinda Z Li, Madian Khabza, Han Fang, and Hao Ma. 2020. Linformer: Self-attention with linear complexity. *arXiv preprint arXiv:2006.04768* (2020).
- [43] Wenjie Wang, Yiyang Xu, Fuli Feng, Xinyu Lin, Xiangnan He, and Tat-Seng Chua. 2023. Diffusion recommender model. In *SIGIR*. 832–841.
- [44] Xiang Wang, Xiangnan He, Meng Wang, Fuli Feng, and Tat-Seng Chua. 2019. Neural graph collaborative filtering. In *SIGIR*. 165–174.
- [45] Jiancan Wu, Xiang Wang, Fuli Feng, Xiangnan He, Liang Chen, Jianxun Lian, and Xing Xie. 2021. Self-supervised graph learning for recommendation. In *SIGIR*. 726–735.
- [46] Qiong Wu, Yong Liu, Chunyan Miao, Binqiang Zhao, Yin Zhao, and Lu Guan. 2019. PD-GAN: Adversarial learning for personalized diversity-promoting recommendation. In *IJCAI*. 3870–3876.
- [47] Yao Wu, Christopher DuBois, Alice X Zheng, and Martin Ester. 2016. Collaborative denoising auto-encoders for top-N recommender systems. In *WSDM*. 153–162.
- [48] Zihao Wu, Xin Wang, Hong Chen, Kaidong Li, Yi Han, Lifeng Sun, and Wenwu Zhu. 2023. Diff4Rec: Sequential recommendation with curriculum-scheduled diffusion augmentation. In *MM*. 9329–9335.
- [49] Jheng-Hong Yang, Chih-Ming Chen, Chuan-Ju Wang, and Ming-Feng Tsai. 2018. HOP-Rec: High-order proximity for implicit recommendation. In *RecSys*. 140–144.
- [50] Zhengyi Yang, Jiancan Wu, Zhicai Wang, Xiang Wang, Yancheng Yuan, and Xiangnan He. 2023. Generate what you prefer: Reshaping sequential recommendation via guided diffusion. In *NeurIPS*.
- [51] Guorui Zhou, Xiaoqiang Zhu, Chenru Song, Ying Fan, Han Zhu, Xiao Ma, Yanghui Yan, Junqi Jin, Han Li, and Kun Gai. 2018. Deep interest network for click-through rate prediction. In *KDD*. 1059–1068.